journal of the mechanical behavior of biomedical materials 138 (2023) 105579

Contents lists available at ScienceDirect

Journal of the Mechanical Behavior of Biomedical Materials

journal homepage: www.elsevier.com/locate/jmbbm

Image quality and scan time optimisation for *in situ* phase contrast x-ray tomography of the intervertebral disc

C.M. Disney [a,b,*], N.T. Vo [b,c], A.J. Bodey [b], B.K. Bay [d], P.D. Lee [a]

[a] Mechanical Engineering, University College London, UK
[b] Diamond Light Source, UK
[c] National Synchrotron Light Source II, Brookhaven National Laboratory, USA
[d] School of Mechanical, Industrial & Manufacturing Engineering, Oregon State University, USA

A B S T R A C T

In-line phase contrast synchrotron tomography combined with *in situ* mechanical loading enables the characterisation of soft tissue micromechanics via digital volume correlation (DVC) within whole organs. Optimising scan time is important for reducing radiation dose from multiple scans and to limit sample movement during acquisition. Also, although contrasted edges provided by in-line phase contrast tomography of soft tissues are useful for DVC, the effect of phase contrast imaging on its accuracy has yet to be investigated. Due to limited time at synchrotron facilities, scan parameters are often decided during imaging and their effect on DVC accuracy is not fully understood. Here, we used previously published data of intervertebral disc phase contrast tomography to evaluate the influence of i) fibrous image texture, ii) number of projections, iii) tomographic reconstruction method, and iv) phase contrast propagation distance on DVC results. A greater understanding of how image texture influences optimal DVC tracking was obtained by visualising objective function mapping, enabling tracking inaccuracies to be identified. When reducing the number of projections, DVC was minimally affected by image high frequency noise but with a compromise in accuracy. Iterative reconstruction methods improved image signal-to-noise and consequently significantly lowered DVC displacement uncertainty. Propagation distance was shown to affect DVC accuracy. Consistent DVC results were achieved within a propagation distance range which provided contrast to the smallest scale features, where; too short a distance provided insufficient features to track, whereas too long led to edge effect inconsistencies, particularly at greater deformations. Although limited to a single sample type and image setup, this study provides general guidelines for future investigations when optimising image quality and scan times for *in situ* phase contrast x-ray tomography of fibrous connective tissues.

1. Introduction

Characterising the structure-function relationship of soft tissues is crucial to solving global healthcare challenges, such as musculoskeletal degeneration and disease. Using x-ray microtomography it is possible to resolve tissue structure in 3D at high resolution (Disney et al., 2017; Walsh et al., 2021). However, soft tissues have low x-ray absorption contrast and so contrast agents or phase contrast techniques are used to resolve microstructure (Rawson et al., 2020; Cianciosi et al., 2021; Arhatari et al., 2021). For instance, in-line propagation-based phase contrast imaging has been used to resolve the microstructure of fibrous connective tissues such as collagen bundles in the intervertebral disc (Disney et al., 2022), tendon (Pierantoni et al., 2021; Sartori et al., 2021) and meniscus (Einarsson et al., 2022), as well as other tissue types such as chondrocyte lacunae in cartilage (Abidin et al., 2018; Tozzi et al., 2020; Madi et al., 2019), and muscle fibres (Borg et al., 2019; Zeller-Plumhoff et al., 2017). *In situ* sample deformation, captured by a series of tomograms during mechanical loading allows micro-to-nanoscale strains to be measured using digital volume correlation (DVC) (Disney et al., 2019; Arora et al., 2017; Sartori et al., 2021; Tozzi et al., 2020). For such micromechanical *in situ* studies, it is important for tissue to maintain its physiological properties and hence, phase contrast techniques without the use of stains are favourable (Disney et al., 2018; Einarsson et al., 2022; Pierantoni et al., 2021).

Synchrotron source x-rays offer higher coherence and flux in comparison to standard laboratory sources, allowing for excellent phase contrast imaging and shorter scans. Work towards shorter scan times is still required, since high resolution, phase contrast tomography scans are relatively long (seconds-to-minutes) in comparison to soft tissue biomechanics which occurs on the order of milliseconds-to-seconds. Consequently, studies are currently limited to quasi-dynamic experiments where scans are only acquired after sample relaxation to avoid

Abbreviations: IVD, Intervertebral disc; DVC, Digital volume correlation; FBP, Filtered back projection; AF, Annulus fibrosus; NP, Nucleus pulposus; SIRT, Simultaneous iterative reconstruction technique; CGLS, Conjugate gradient for least squares.

* Corresponding author. Diamond Light Source, Harwell Science and Innovation Campus, Didcot, Oxfordshire, OX11 0DE, UK.
E-mail address: catherine.disney@diamond.ac.uk (C.M. Disney).

https://doi.org/10.1016/j.jmbbm.2022.105579
Received 15 August 2022; Received in revised form 14 November 2022; Accepted 16 November 2022
Available online 19 November 2022

movement artefacts in the reconstructed image. Furthermore, samples are subjected to high levels of radiation since multiple scans are required. Few studies have attempted to quantify the effect of radiation damage on biological samples from synchrotron tomography, which is particularly important for *in situ* experiments involving tissue mechanics and DVC measurements. Seminal work by Barth et al. (2011) found that high radiation dose caused embrittlement of bone which were linked to changes in collagen molecular structure and crosslinking. As a result, x-ray tomography studies have since used 35 kGy as a reference point (Dall'Ara et al., 2022). Besides the crack formations observed by Barth et al. development of local strains have also been detected in bone during repeat tomography scans (Fernández et al., 2018). Although these changes were found in bone and not soft tissue, they demonstrate the importance and need for reducing radiation dose for mechanical *in situ* studies.

In this study, two scan parameters – number of projections and phase contrast propagation distance – and reconstruction methods are explored to optimise image quality and scan time for *in situ* DVC studies of fibrous connective tissues using previously published data on the intervertebral disc (Disney et al., 2022). Both number of projections and propagation distance are often decided empirically during data collection. For example, a series of scans are taken with increasing projections or increasing propagation distance, then the chosen parameters are decided by visual inspection of a reconstruction or post hoc image quality quantification (Strotton et al., 2018; Disney et al., 2019). Due to limited data collection time during synchrotron tomography studies, quantitative evaluation is often neglected with parameters selected based on qualitative judgement. Here, we aim to quantify the effect of these parameters on image quality and DVC analysis to optimise scans for analysis.

Many projections are required to reconstruct an image volume, typically achieved using filtered back projection (FBP) methods. The Nyquist sampling theorem gives the theoretical optimal number of projections required for reconstruction (Kak and Slaney, 2001).

$$N = N_p \times \frac{\pi}{2} \tag{1}$$

Where N is number of projections and N_p is number of pixels at the widest horizontal part of the sample. Under-sampling causes aliasing artefacts and lower signal-to-noise (but it may still be possible to resolve structures) whereas oversampling provides overlapping and summation of signal, gaining some improvements in signal-to-noise and reducing the effect of artefacts from experimental factors. Iterative reconstruction methods have been developed and applied to improve signal-to-noise in scans with a low number of projections (Kak and Slaney, 2001). Thus, this study aims to optimise the number of projections required for tomography and DVC analysis using FBP and iterative reconstruction methods.

In-line phase contrast imaging is dependent on the propagation (sample-to-detector) distance and x-ray energy. With sufficient propagation of the beam from the sample, Fresnel fringes appear at the edge of structures, increasing their contrast. Edge enhancement of structures is given by the following relationship (Burvall et al., 2011)

$$Z \sim \frac{a^2}{\lambda} \tag{2}$$

Where Z is the propagation distance of the beam from the sample, a is the dimension of the scattering object and λ the x-ray wavelength. However, this is an approximate relationship which can be fine-tuned to optimise the resulting contrast-to-noise in the reconstructed image volume (Lovric et al., 2013). Increasing this distance causes the near-field edges to become brighter but more blurred. The relationship between level-of-edge-enhancement from in-line phase contrast, image quality and DVC accuracy has previously not been quantified. Therefore, this study aims to investigate how various level-of-edge-enhancement from in-line phase contrast tomography affects the accuracy of DVC analysis.

The local approach of DVC involves creating a point cloud which defines the centre of sub-volumes used to correlate between image volumes, by the optimisation of normalised sum-squared-difference function. The size of sub-volumes is also chosen empirically where displacement uncertainty is quantified from zero-strain repeat tomography scans (Tozzi et al., 2020; Wearne et al., 2022; Tavana et al., 2020; Gates et al., 2015). Larger sub-volumes tend to be more reliable but cover a larger volume and so have lower tracking resolution, whereas smaller sub-volumes may have insufficient texture for accurate tracking (Palanca et al., 2015). Synchrotron tomography offers high resolution imaging, and so with the appropriate sub-volume size and management of point cloud, nanoscale measurements are achievable (Madi et al., 2019). Quantifying displacement uncertainty and optimising DVC parameters such as sub-volume size from zero-strain repeat scans is therefore important when investigating the effect of image quality on DVC analysis (Dall'Ara et al., 2022; Pan and Wang, 2020).

Many musculoskeletal tissues have a predominating fibrous structure, which means that the resolved image texture often has long-narrow repeating features (Disney et al., 2022; Sartori et al., 2021). Understanding the influence of resolved image texture, such as by fibres, on DVC analysis should therefore be considered. Here, we used two approaches; objective function mapping to characterise the optimisation problem and fibre fitting methods, to identify where DVC tracking may be inaccurate.

In summary, this study aimed to evaluate the effect of four factors (image texture, the number of projections, reconstruction methods, and propagation distance for phase contrast imaging) on image quality and DVC performance.

2. Methods

2.1. In situ phase contrast synchrotron CT of intervertebral disc

The image data used here was collected at the Imaging and Coherence beamline (I13-2) at Diamond Light Source. Only brief imaging methods are described here, however full details can be found in (Disney et al., 2022). A Sprague Dawley rat spine segment mounted in a Deben CT5000 rig for *in situ* compression was used (Fig. 1a and b). The sample was studied during four cumulative compression steps of 0.02 mm each (~2% strain). A scan was taken after each compression step and stress relaxation to produce a series of image volumes of the compressed spine segments. A total of 8001 projections with field-of-view of 4.2 × 3.5 mm and 1.625 μm pixel size were taken. Propagation distance between the sample and detector was set empirically to 0.35 m to achieve sufficient phase contrast in the reconstructed volumes.

2.2. Radiation dose calculation

Absorbed energy was calculated based on a mean energy of 27.6 keV (4.42×10^{-15} J). The sample absorption coefficient of 0.167 was estimated by using a transmission calculation (https://henke.lbl.gov/optical_constants/filter2.html, last accessed October 2022) (Henke et al., 1993), assuming H_2O composition, density 1 gcm^{-3} and thickness of 5 mm. Thus, absorbed flux is given as beam flux multiplied by the absorption coefficient (1×10^{12} x $0.167 = 1.67 \times 10^{11}$ photons s^{-1} mm^{-2}) and absorbed energy flux given by mean energy and absorbed flux ($4.42 \times 10^{-15} \times 1.67 \times 10^{11} = 7.4 \times 10^{-4}$ J s^{-1} mm^{-2}). Total exposure time is given by the number of projections, 0.15 s exposure and 10 ms overhead per projection (8001*(0.15 + 0.01) = 1280.16 s).

Dose was estimated as

$$Dose\ (Gy) = \frac{Exposure\ time\ (s) \times Absorbed\ energy\ flux\ \left(\frac{J}{sm^2}\right)}{Mass\ per\ unit\ area\ \left(\frac{kg}{m^2}\right)} \tag{3}$$

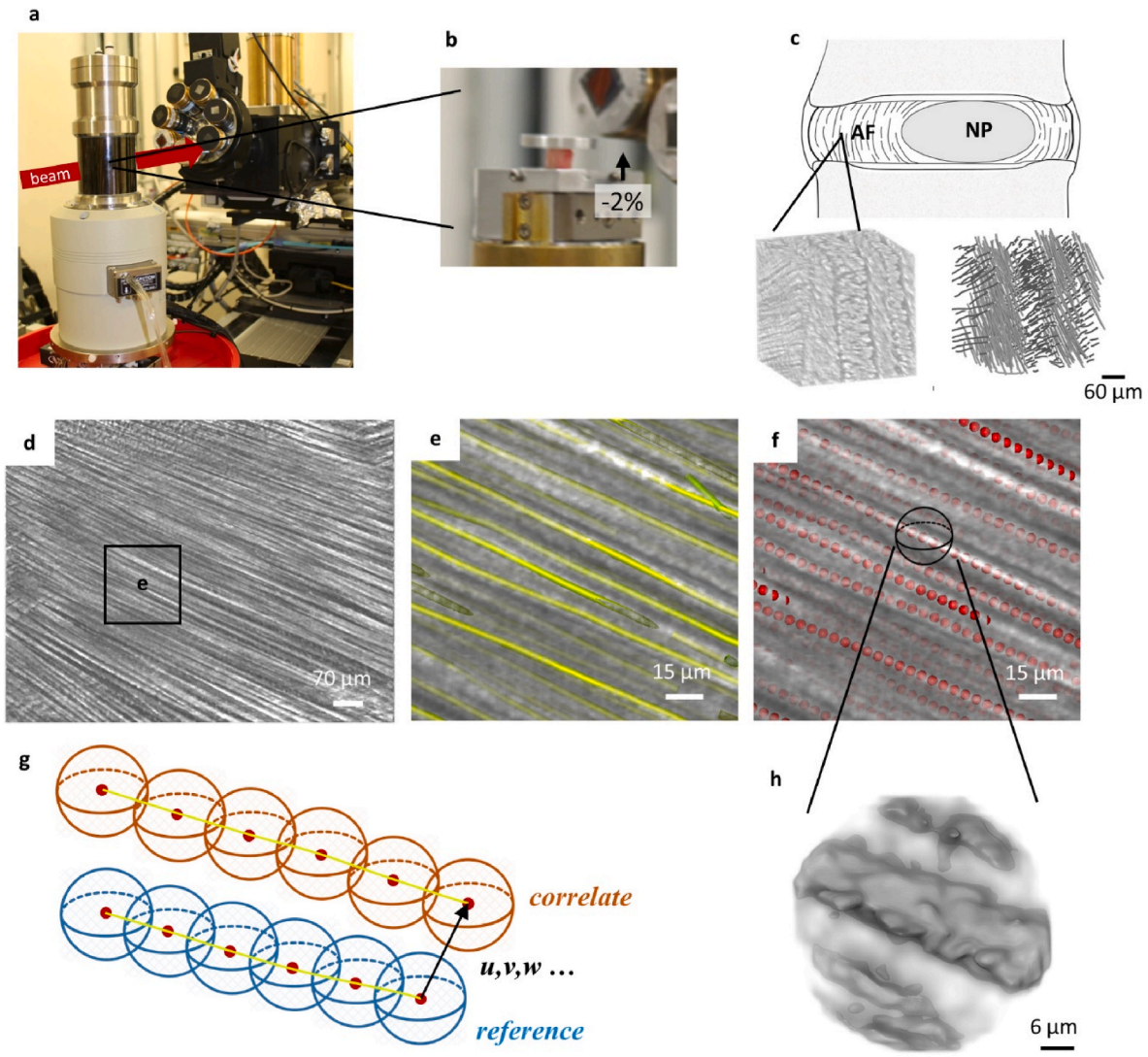

Fig. 1. ***In situ*** **analysis set up. a)** Beamline setup with rig in place. **b)** Sample placement within the rig. 2% compression steps were applied from the bottom plate and scans were taken after each compression step. **c)** Schematic of the intervertebral disc anatomy including the annulus fibrosus (AF) and nucleus pulposus (NP). Regions of interest were taken from scans in the fibrous AF. **d)** Example slice taken from a tomogram showing fibres resolved in the AF. **e)** Traced fibres in the same example slice. **f)** Points seeded along each traced fibre to create a fibre-based point cloud for DVC analysis (**g**). **h)** Each point represented a sub-volume which was correlated between image volumes.

The dose for 8001 projection scan was calculated as 189 kGy.

2.3. Reconstructions

All image volumes were reconstructed using the Python package Algotom (https://algotom.readthedocs.io) (Vo et al., 2021). Scripts included steps to pre-process data by applying flat-field correction, distortion correction (Vo et al., 2015), ring artefact removal (Vo et al., 2018) and zinger removal before each reconstruction. FBP was performed for 8001, 7000, 6000, 5334, 4000, 2667, 2000 and 1000 projections sampled evenly across 180°. For comparison purposes, reconstructions are referred to by their number of projections relative to the theoretical number of projections from the sampling theorem in eq. (1).

$$\varphi = N_r / \left(N_p \times \frac{\pi}{2} \right) \tag{4}$$

Where N_r is number of projections used in the reconstruction. Hence, reconstructions with 8001, 7000, 6000, 5334, 4000, 2667, 2000 and 1000 projections have φ values 2, 1.75, 1.5, 1.33, 1, 0.66, 0.5, 0.25 respectively.

Repeat scan reconstructions were created by sampling different projections for each image volume. Iterative reconstructions of 2000 projections ($\varphi = 0.5$) using simultaneous iterative reconstruction technique (SIRT) and conjugate gradient for least squares (CGLS) was also applied (Vo et al., 2021; Van Aarle et al., 2016).

Different propagation distances were simulated for repeat scan reconstructions by using the original measured condition (27.6 keV energy, 1.625 µm pixel size, 350 mm propagation distance) and a Fresnel propagator to estimate phase and absorption contribution (Vo et al., 2012).

2.4. Digital volume correlation

Point clouds were created by either, distributing evenly spaced points throughout the volume of interest, or by evenly seeding points every 5 voxels (8 µm) along each traced fibre, resulting in over 43,000 points along >1500 fibres (Fig. 1d–f, 2a-b).

Open-source DVC code supported by the Collaborative Computational Project in Tomographic Imaging (CCPi) was used (https://tomo

graphicimaging.github.io/iDVC, last accessed October 2022) (Disney et al., 2022). Sub-volumes were defined as spheres with sampling points randomly distributed within a specified diameter. Grey levels were interpolated within sub-volumes at these points to allow sub-voxel displacement measurements (Fig. 1h). A high number of sub-volume sampling points (10,000) and a tricubic interpolator was used for all analysis. A normalised-sum-squared-difference objective function was minimised by a nonlinear least-squares optimisation using 12 degrees of freedom – translation, rotation, and linear strain. Points ran in distance order from an initial manually registered point with forward transfer of parameters as starting estimates for neighbouring points. Lagrange strain was calculated using the derivative of local neighbourhood

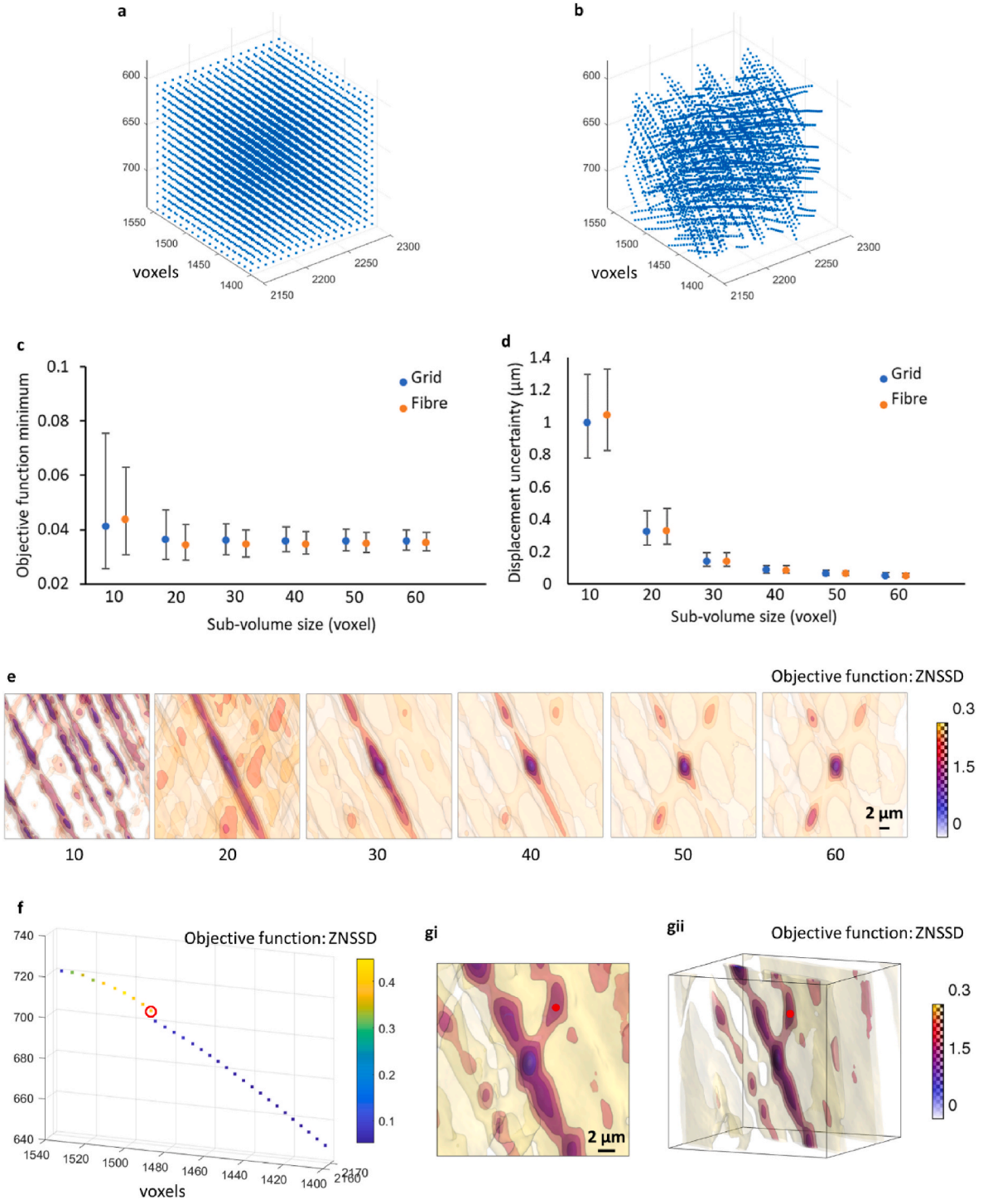

Fig. 2. Optimisation of sub-volume size is dependent on structure size and shape. a) Point cloud arranged as evenly spaced grid. **b)** Point cloud based on fibre tracing. **c)** Median and interquartile range of minimum objective function values for a range of sub-volume sizes. **d)** Median and interquartile range of measured displacement uncertainty for a range of sub-volume sizes. **e)** Objective function map for a single point with various sub-volume sizes viewed from the transverse plane. Each search volume was set to 20 voxels cubed using 100 point locations cubed. **f)** Example of a single fibre's tracked points coloured by objective minimum. The circled point indicates where tracking was lost to a local minima located at an adjacent fibre. **g)** Objective function mapping of the circled point in f), where the red dot marks the location of tracked point to a local minima.

displacements fitted to third order polynomials. Displacement and strain uncertainties were found by using zero-strain repeat scans.

Objective function values were mapped across the search area to visualise the optimisation problem for a single point. The objective function was calculated at 100^3 points evenly distributed across a 20^3 voxel search area. Iso-surface renderings were used to plot the objective function maps using Avizo 3D (version 2021.1, Thermo Fisher Scientific).

2.5. Image analysis

Signal-to-noise and contrast-to-noise ratios were calculated to quantify image quality. Signal-to-noise was calculated as the mean grey value within the intervertebral disc sample AF ($\overline{X}_{AF}$) divided by the standard deviation of the background grey values (outside of the sample, $\overline{X}_o$) (Pacureanu et al., 2012).

$$SNR = \overline{X}_{AF} / \overline{X}_o \tag{5}$$

Contrast-to-noise was quantified by the difference in sample and background mean grey values divided by the standard deviation of the background grey values (σ_o) (Hahn et al., 2012).

$$CNR = (\overline{X}_{AF} - \overline{X}_o) / \sigma_o \tag{6}$$

The same 200^3 voxel regions across reconstructions were used for the signal- and contrast-to-noise calculations.

Fibres were traced using the XFiber Avizo 3D extension (version 2021.1, Thermo Fisher Scientific). This package correlated a cylinder template to the image data and then traced fibres at a chosen confidence level (>80).

2.6. Statistical methods

Points belonging to each fibre were fitted to cubic parametric space curve equations. The goodness-of-fit (residual and r-squared) values were used to identify where DVC may have inaccurate tracking.

A multiple comparison ANOVA test was used to show significant differences between DVC results. Full comparison tables can be found in the supplementary information.

3. Results and discussion

3.1. Influence of image texture on DVC analysis

Image texture is used to track displacements, and therefore it is important to consider the scale and type of features resolved in image volumes when setting up DVC analysis. Sub-volume size is typically decided empirically by objective function values and measuring displacement uncertainty from zero-strain repeat scans (Fig. 2c and d) (Disney et al., 2022; Tozzi et al., 2020; Dall'Ara et al., 2017; Wearne et al., 2022; Tavana et al., 2020; Gates et al., 2015). Distribution of the objective function values gives some indication of successful tracking – lower values with a narrow distribution for larger sub-volumes suggests reliable displacement tracking whereas a wider distribution towards higher values for smaller sub-volumes suggests unsuccessful tracking. Loss of tracking for small sub-volumes is generally due to insufficient image texture or lack of unique features for correlation. In these cases, optimisation can be to a local minimum indicated by higher displacement uncertainty values e.g., sub-volume sizes 10 and 20 in Fig. 2c and d.

Mapping objective function values over the search region reveals the importance of image texture when selecting sub-volume size (Fig. 2e). Fig. 2e shows the objective function map for sub-volumes 50 and 60. The larger 50–60 voxel sub-volumes include microstructural detail from 2 to 3 fibres resulting in a defined global minimum with separation from local minima. As sub-volume size is decreased, to only include the edges of a single fibre, optimisation tends to a long narrow valley located along the fibre. Local optima solutions are more likely if the valley has a long, shallow gradient along the fibre (Fig. 2e, sub-volume size 20). Sub-volumes which do not include sufficient texture, such as the edge of the fibre, may have no defined global minimum (Fig. 2e, sub-volume size 10).

Fig. 2 f-g shows an example of when the global minimum did not have clear separation from a local minimum, resulting in inaccurate tracking. In this case, tracking has hopped across to an adjacent fibre. However, it is possible to identify this by looking for changes in objective minimum values, abrupt changes in displacement along the fibre, and lower fibre goodness-of-fit (r-square and residual values from space curve fitting) (Disney et al., 2022).

Although it is widely accepted that sub-volume size should be decided from zero-strain DVC analysis (Dall'Ara et al., 2022), the underlying reason is rarely investigated. Here, we have shown that tracking can be lost due to long narrow valley optimisation or local optima on adjacent features. With this further understanding of how these inaccuracies occur it is possible to identify them and discount them from the final results. From the example given in Fig. 2f, points which ran subsequently after the lost tracking were also affected which may be due to forward transfer of parameters as starting estimates. Future work could include automatically identifying when tracking is lost and adjusting new input estimates from the local neighbourhood average.

3.2. Optimising number of projections

Previous DVC accuracy studies show that there is a trade-off between scan time and compromising DVC accuracy for *in situ* measurement (Dall'Ara et al., 2022; Fernández et al., 2018; Madi et al., 2019). Synchrotron tomography offers fast, high-resolution imaging but at high radiation dose, in this case estimated as over 189 kGy for one scan with 8001 projections ($\varphi = 2$). Barth et al. (2011) found that high radiation doses (above 35 kGy) caused embrittlement due to collagen I fragmentation and crosslinking in their bone samples. Although their study was in bone, which is highly absorbent to x-rays, they also discuss commonalities in damage mechanisms which occurred in tendon gamma radiation studies (another form of ionising radiation). Cartilage has shown decrease in compressive stiffness and reduced proteoglycan levels after being irradiated with low doses of ionising radiation (Lindburg et al., 2013; Cicek, 2016). More work is required to study the effect of synchrotron radiation on soft tissues (such as tendon, cartilage and intervertebral disc), however these studies provide some guidance on 'safe' levels of irradiation and reassert the importance of lowering scan time through number of projections. Image quality was observed from FBP reconstructed volumes (Fig. 3a). An increased level of noise was seen for reconstructions below $\varphi = 1$. Reconstruction artefacts appeared in volumes with fewer projections ($\varphi = 0.25$). Image quality was quantified using signal-to-noise and contrast-to-noise ratios. As expected, these values considerably dropped for reconstructions with projections less than $\varphi = 1$ (Fig. 3b). High signal- and contrast-to-noise ratios were found for reconstructions above $\varphi = 1.25$. An increase in signal-to-noise for reconstructions with projections above $\varphi = 1$ was due to averaging of the signal. This can be useful in cases where there are artefacts or noisy regions which are characteristic of the sample. Here, for example, the calcified endplate has high absorption in comparison to the soft tissue, causing streaks and noise (Disney et al., 2019, 2022).

Importantly, we must consider if such high-resolution imaging using many projections is required to carry out quantitative analysis. Fibre tracing was used to quantify how well-resolved the microstructure was. Fig. 3c shows the relative difference in the confidence level of tracking fibres. A total of ~30% difference was found between reconstructions $\varphi = 1.5$ and $\varphi = 0.5$, following a similar trend to signal- and contrast-to-noise quantification.

Simulated zero-strain repeat tomography from evenly sampled projections was used to evaluate the effect of number of projections on DVC

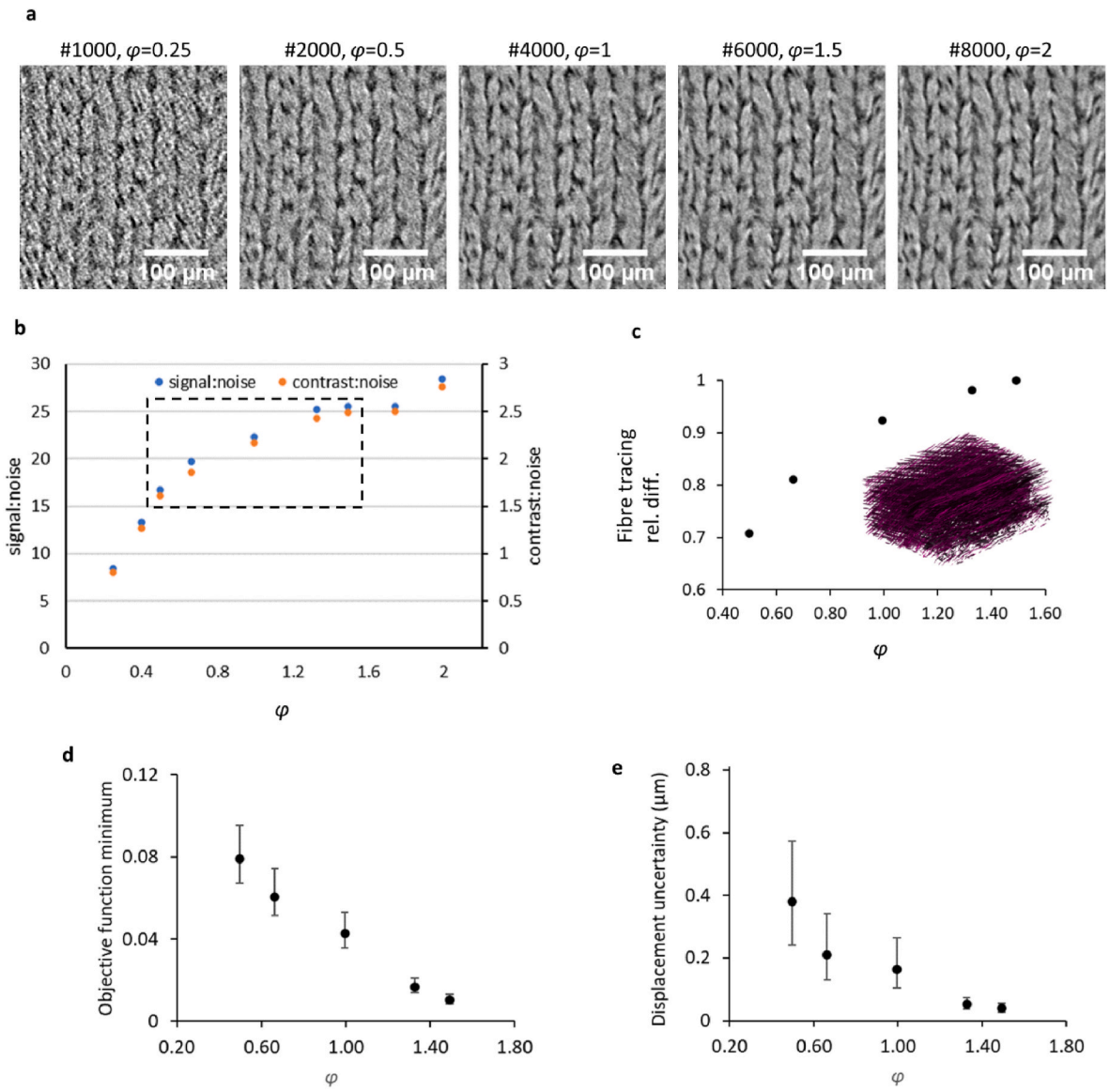

Fig. 3. Optimising number of projections for DVC. a) intervertebral disc AF structures resolved using FBP reconstruction with different number of projections. **b)** Signal- and contrast-to-noise ratios of image volumes reconstructed using different number of projections. Box indicates number of projections used in further analysis (fibre tracing and DVC). **c)** Relative difference in fibre tracing confidence level (voxels >80) for reconstructions with different number of projections. **d)** Mean and interquartile range of objective minimum values for DVC zero-strain analysis of reconstructions with different number of projections. **e)** Mean and interquartile range of displacement uncertainty for zero-strain DVC analysis of reconstructions with different number of projections.

analysis (Fig. 3d and e). Objective function values gave some indication of how consistent and how suitable the resolved texture was for correlation. There was a negative, linear trend between increasing number of projections used in reconstruction and median objective function value. This means that correlation benefits from the higher signal-to-noise ratio of reconstructions with more projections.

However, it was important to quantify how reliable and accurate tracking was for different reconstructions using displacement uncertainty from zero-strain DVC. Median displacement uncertainty was low, below 0.2 μm, for reconstructions with number of projections $\varphi \geq 0.66$ and thus achieved high accuracy tracking. The distribution of displacement uncertainty values can be used to indicate reliability of tracking. The larger the distribution, the less reliable tracking is likely to be. Nonetheless, all tracking points for reconstruction with $\varphi = 0.66$ projections (approximately 63 kGy) had displacement uncertainty less than 0.55 μm, equivalent to ~1/3 a voxel accuracy, and so are considered to be reliable and have high accuracy.

Iterative reconstruction can be used to improve image quality when there are a low number of projections acquired (Kak and Slaney, 2001). Fig. 4a and b shows the image quality obtained for two different iterative reconstruction methods versus FBP for $\varphi = 0.5$ projections (lowering radiation dose to approximately 47 kGy). Iterative reconstruction methods increased signal- and contrast-to-noise ratios to a value almost equivalent to FBP $\varphi = 1.5$. The optimum signal- and contrast-to noise ratios using SIRT reconstruction was found after 50 iterations and so the reconstruction with 10 iterations was discounted from further DVC analysis. A notably lower level of high frequency noise was observed in reconstructed image volumes when compared to FBP. However, with increasing number of iterations, signal only slightly improved whereas noise considerably increased, causing a subsequent decrease in signal-to-noise ratio (Fig. 4c). We hypothesise that, with a higher number of iterations, it may be possible to resolve the more detailed image texture required for improved DVC accuracy, but, there is also an increase in noise from highly absorbing structures (e.g. calcified endplate) (Croton et al., 2018; Disney et al., 2022). Future work may consider using alternative reconstruction methods which aim to reduce

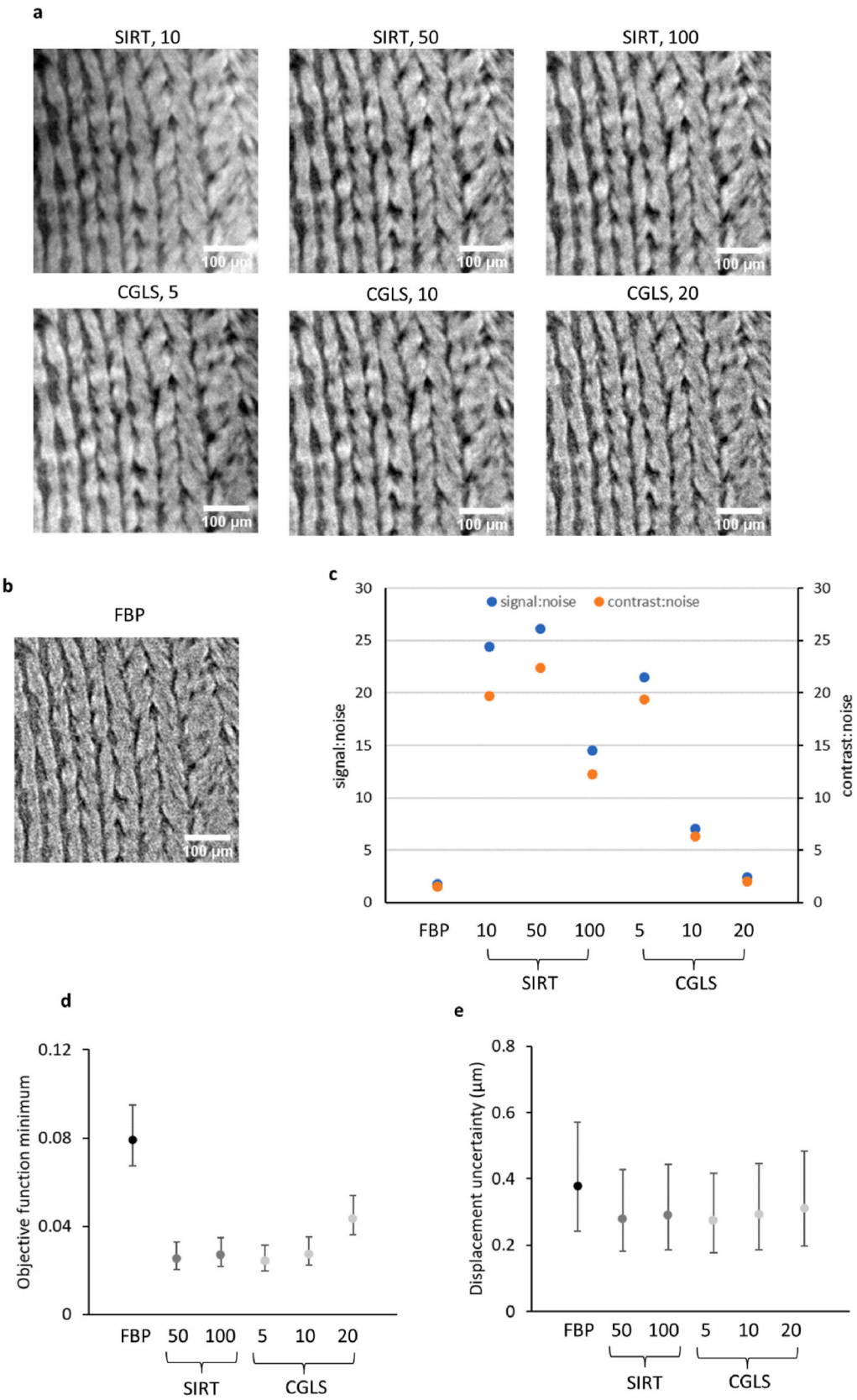

Fig. 4. Iterative reconstruction for reduced numbers of projections improves image quality and DVC accuracy a) Comparison of intervertebral disc AF structures resolved using SIRT and CGLS with a different number of iterations. **b)** Same region shown the reconstructed image using FBP. **c)** Contrast- and signal-to-noise comparison between the different reconstruction methods. **d)** Median and interquartile range of objective minimum values for zero-strain DVC accuracy analysis for the different reconstruction methods. **e)** Median and interquartile range of displacement uncertainty for DVC analysis of the different reconstruction methods. Iterative reconstruction methods significantly improved displacement accuracy ($p < 0.001$, multiple comparison ANOVA) when compared to FBP.

these artefacts (Boas and Fleischmann, 2011; Hehn et al., 2018).

DVC objective function and displacement uncertainty values from iterative and FBP reconstructions are shown in Fig. 4 d-e. There was significant improvement in objective function and displacement uncertainty values using iterative reconstruction methods for $\varphi = 0.5$ (See Suppl. info. for full comparative testing). An estimated dose of 47 kGy is still considered high and so there is still further work to be done in lowering radiation dose whilst maintaining sub-micron DVC accuracy. It is vital to consider other factors which contributed to the longer scan times and higher dose in our study. For instance, Pierantoni et al. (2021) had similar imaging parameters (2000 projections, field-of-view, 1.6 μm pixel size) and a comparable dose rate (200 Gy/s) to this study (148 Gy/s) but they achieved considerably lower dose per tomogram (18 kGy) due to a shorter projection overhead time.

Choosing an iterative reconstruction method over FBP greatly improved image quality which is useful for image processing, however it only moderately improved DVC accuracy. DVC requires small scale features for high accuracy tracking. Less than 2000 projections resulted in aliasing artefacts which had a similar scale and intensity to the microstructure used in DVC. Since these types of artefacts lead to DVC inaccuracies, these reconstructions have not been included.

3.3. Effect of propagation-based phase contrast on DVC accuracy

Figs. 5–6 show the first results exploring the influence of in-line phase contrast on the accuracy of measuring tissue deformation using DVC. In-line phase contrast, used to resolve soft tissue microstructure, creates highly contrasted edges which are particularly useful for DVC (Tozzi et al., 2020; Madi et al., 2019; Disney et al., 2022). The amount of propagation distance can be fine-tuned and is typically decided empirically during an experiment (Strotton et al., 2018; Pierantoni et al., 2021; Lovric et al., 2013). Reconstruction results simulating different propagation distances are shown in Fig. 5a. With increasing propagation distance, a brighter edge effect was observed, and so contrast-to-noise

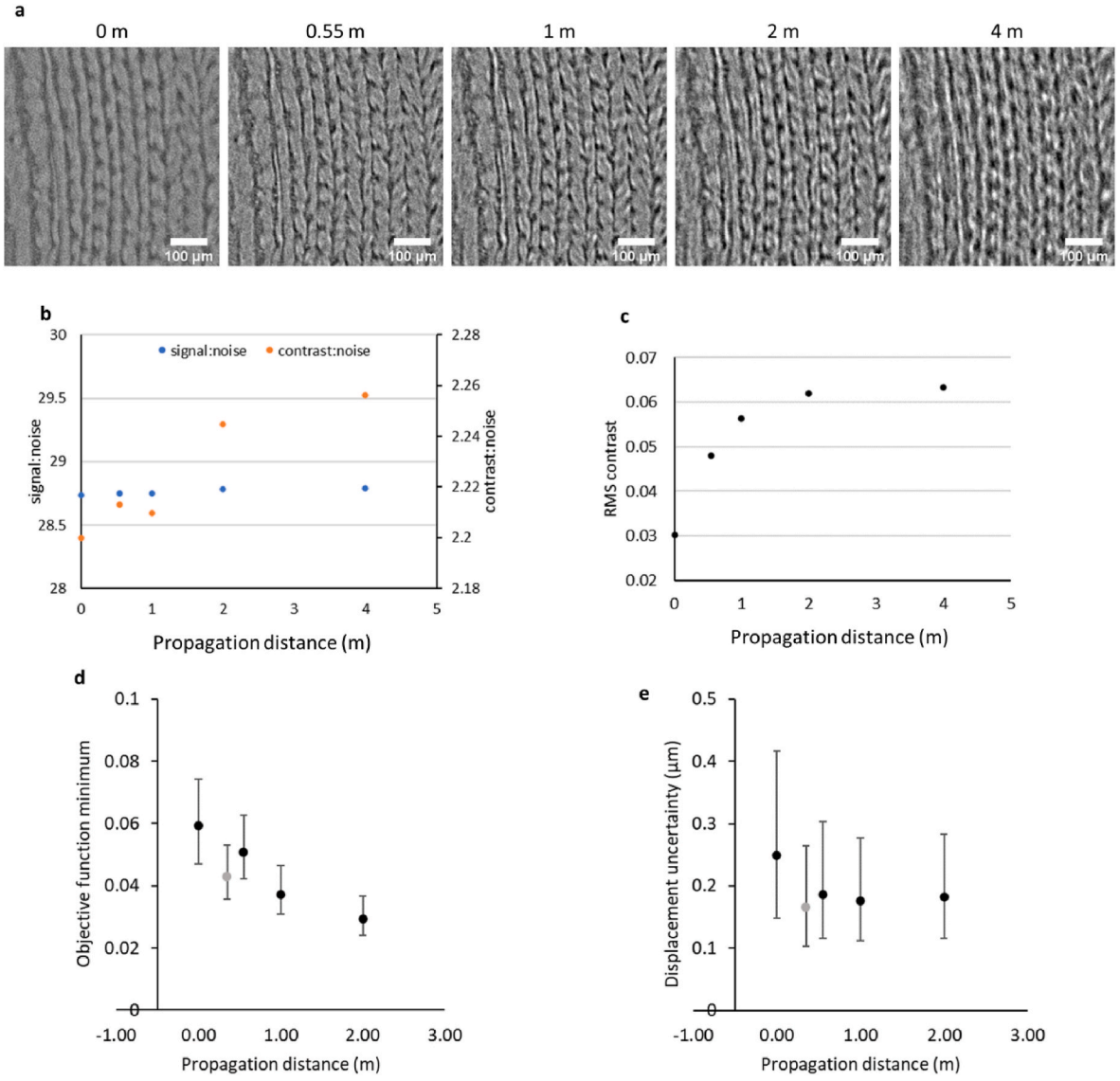

Fig. 5. Effect of phase contrast on zero-strain DVC. a) Comparison of structures resolved using different propagation distances. **b)** Comparison of contrast- and signal-to-noise for reconstructions with different simulated propagation distances. **c)** RMS (root means square) contrast measured for each reconstruction at different simulated propagation distances. **d)** Median and interquartile range of objective minimum values for zero-strain DVC accuracy analysis. **e)** Median and interquartile range of displacement uncertainty for zero-strain DVC. Displacement uncertainty was not significantly different ($p < 0.001$, multiple comparison ANOVA) between propagation distance 1 and 2 m, all other comparisons were significantly different. Black markers indicate the simulated reconstructions (0, 0.55, 1, 2 m) and grey the experimental data (0.35 m).

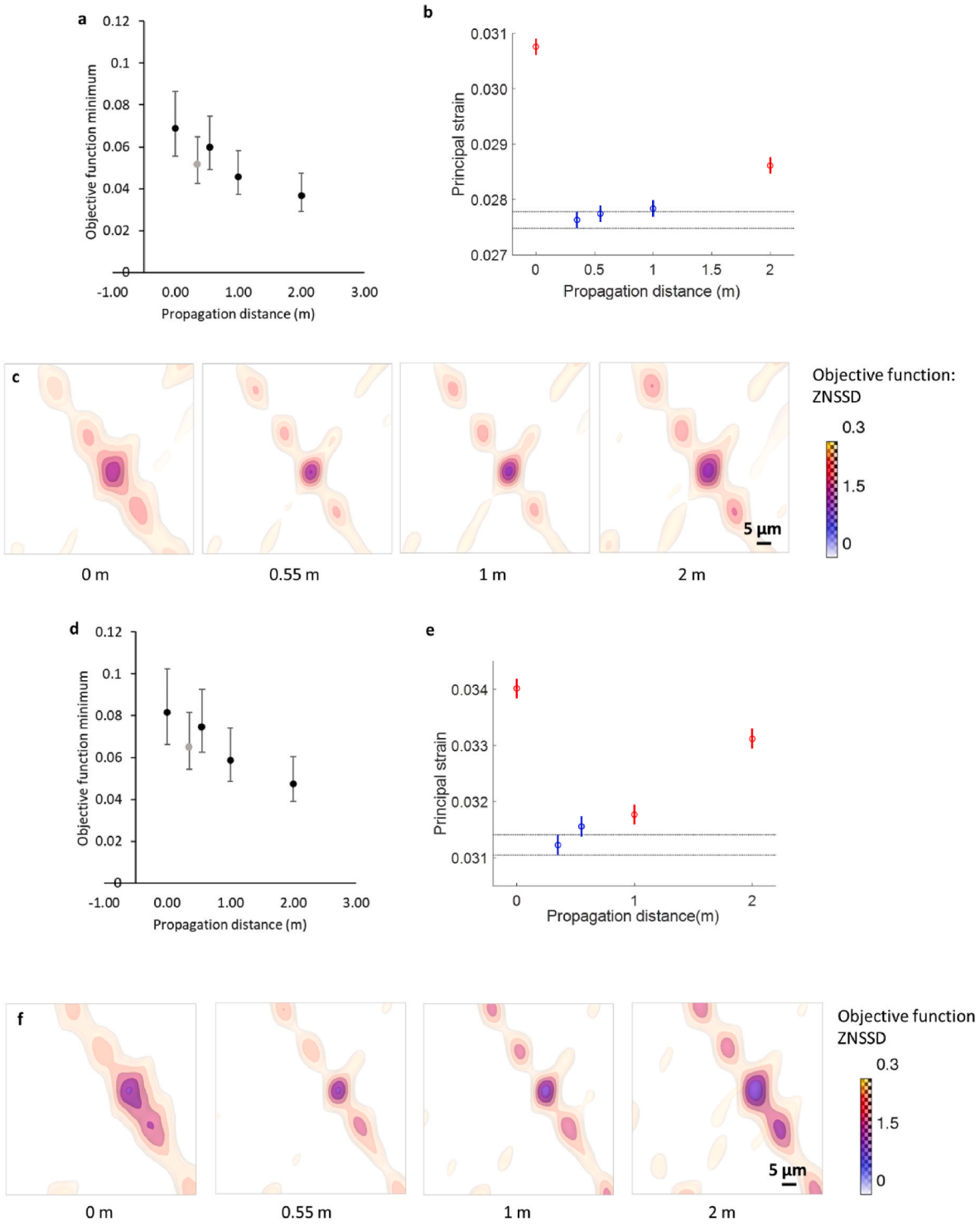

Fig. 6. Effect of phase contrast imaging on *in situ* DVC measurement for 2% applied strain (a,b,c) and 4% applied strain (d,e,f). a) Median and interquartile range of objective minimum values for different propagation distances for 2% applied strain. Black markers indicate the simulated reconstructions (0, 0.55, 1, 2 m) and grey the experimental data (0.35 m). **b)** Mean and standard error of principal strain values versus propagation distances for 2% applied strain. Multi-comparison between the groups shows that strains are significantly different at 0 m and 2 m propagation distances (red markers, $p < 0.001$, multiple comparison ANOVA). **c)** Objective function mapping of the same point using reconstructions at different propagation distances. **d)** Median and interquartile range of objective minimum values for different propagation distances for 4% applied strain. **e)** Mean and standard error of principal strain values versus propagation distances for 4% applied strain. Multi-comparison analysis between the groups shows that strains are significantly different at 0, 1 and 2 m propagation distances shown as red markers ($p < 0.001$, multiple comparison ANOVA). **f)** Objective function mapping of the same point using reconstructions at different propagation distances for 4% applied strain.

ratio increased (Fig. 5b). The scale of features with higher contrast increased with propagation distance. At 0.55 m, small structures have sharp, high contrast, whereas at 1 and 2 m, the edge effect is more blurred and larger lamellar structures have enhanced edge contrast. At very large distances, such as 4 m, the image no longer represents the microstructure but instead the detector records some far-field diffraction.

The influence of phase contrast propagation distance on zero-strain DVC analysis is shown in Fig. 5 d-e. A decrease in objective function values was associated with larger propagation distance. Highly contrasted textures, such as those simulated at larger propagation distances, are more successful for correlation. There was very little difference in displacement uncertainty for reconstructions with propagation distance above 0 m.

Incremental load steps are used to study a sample's total deformation. The magnitude of load and number of steps is sample- and study-dependent. Experiments are often designed to be conservative so that analyses of the data collected have higher chances of success. For this example, it is expected that the intervertebral disc will have large heterogenous deformations, and so small 2% compression steps (roughly 20 μm, 12.3 pixels) were chosen. Here, we aimed to refine methods by studying the effect of larger load steps, and therefore reduced total number of scans, on accuracy of DVC. It is also unknown how phase contrast imaging will affect the accuracy of results for larger sample deformations.

Displacement uncertainty from zero-strain repeat scans is only a measurement of how successful the resolved texture is for DVC. Little is known about the effect of in-line phase contrast on DVC accuracy in measuring tissue deformation. One hypothesis could be that, since propagation phase contrast is related to feature size, when the sample is deformed, microstructural features change which alter the resolution of image texture tracked between tomography reconstructions. Fig. 6 compares DVC results for different propagation distances and two load levels (2% and 4% compression). As in Fig. 5, median objective minimum value decreases with increasing propagation distance, as expected with highly contrasted image volumes (Fig. 6a). A multiple comparison ANOVA test revealed that principal strain values for reconstructions at the longer simulated distances of 0 m and 2 m were significantly different to all other analyses (Fig. 6b). Reconstructions simulated at 0 m and 2 m had a higher principal strain mean and standard deviation suggesting lower accuracy. When comparing objective function maps, closer iso-surfaces and therefore steeper gradients were observed using 0.55 m and 1 m reconstructions when compared to 0 and 2 m. These steeper gradients are more favourable for optimisation. Blurring or changes with load at the edges of structures with increased propagation phase contrast, such as at 2 m, are likely responsible for the differences in objective function gradient.

With an increased load of 4% compression, the median objective function followed the same trend as the lower 2% load, but with an overall higher value (Fig. 6d). A multiple comparison ANOVA test for increased load (4%) revealed that principal strain values for propagation distances 0, 1 and 2 m were significantly different compared to the experimental data (0.35 m) and 0.55 m.

Overall, the results in Fig. 6 show that the optimised propagation distance range lies where there is sufficient contrast to resolve the smallest scale features. Below this range, there is insufficient image texture to track, whereas above this range, the bright edges affect the DVC results. This optimised range becomes narrower for samples with higher deformation.

4. Conclusions

This study only investigated one type of tissue with consistent texture and so exact findings cannot be directly applied to other studies with different beamline setups and samples. However, the general findings presented are applicable to the *in situ* phase contrast tomography-based study of a wide range of fibrous musculoskeletal tissues, such as tendon, meniscus, and cartilage. Since in-line phase contrast is dependent on the material refractive properties and the feature size, further work is required investigating samples with multiple tissue types, such as soft-calcified tissue boundaries, which may benefit from multiple-distance imaging, multi-material phase retrieval algorithms (Häggmark et al., 2017) or by applying Fresnel propagator (Vo et al., 2012) as done here by simulated reconstructions (Fig. 5a).

Experimentally investigating multiple propagation distances would be extremely challenging due to repeatability of soft tissue biomechanics and so this study was only possible using simulated results. One disadvantage of this is that results may be incomplete, as they are based only on the information provided in the experimental data, at 0.35 m propagation distance.

There are many contributing factors which can affect radiation dose, image quality and the accuracy of DVC measurement, such as sample composition and microstructure, beam energy, exposure time, propagation distance, number of projections, reconstruction algorithm, image filtering before and after reconstruction and, DVC parameters. Here, we only studied a few with the aim of quantifying image quality and DVC accuracy which have been summarised below and in Fig. 7:

1. Our results indicated that there is an optimised range for propagation distance which gives consistent DVC results depending on feature size. Larger applied strain steps, and therefore fewer total scans per experiment, should be considered for low dose studies at shorter propagation distances. As this is the first study of the effect of phase contrast imaging on DVC accuracy, future work should investigate phase retrieval methods for multi-material tomography.
2. Scans at the highest resolution, with many projections, are not required for DVC, since measurement was robust to high frequency image noise in reconstructions with fewer projections, but with some compromise in accuracy. Although this study has shown it is possible to reduce radiation dose through shorter scans, future work is also required to quantify radiation damage of tissue at different length scales (i.e. tissue and protein).
3. Iterative reconstruction methods improved signal-to-noise and lowered DVC displacement uncertainty. The challenges for *in situ* tomography biomechanics also include optimising reconstruction for samples with soft-hard tissue to reduce dominant streaking artefacts from absorption mismatch.
4. DVC parameters such as sub-volume size must be optimised for image texture. In future studies, samples with different tissue types and thus varied microstructural texture will likely require tissue-specific DVC parameters, such as sub-volume size, for accurate tracking.

CRediT authorship contribution statement

C.M. Disney: Writing – review & editing, Writing – original draft, Visualization, Validation, Software, Resources, Methodology, Investigation, Formal analysis, Data curation, Conceptualization. **N.T. Vo:** Writing – review & editing, Software, Resources, Methodology. **A.J. Bodey:** Writing – review & editing, Formal analysis, Data curation. **B.K. Bay:** Writing – review & editing, Software, Resources, Methodology, Funding acquisition, Formal analysis, Data curation. **P.D. Lee:** Writing – review & editing, Supervision, Resources, Funding acquisition.

Declaration of competing interest

The authors declare that they have no known competing financial interests or personal relationships that could have appeared to influence the work reported in this paper.

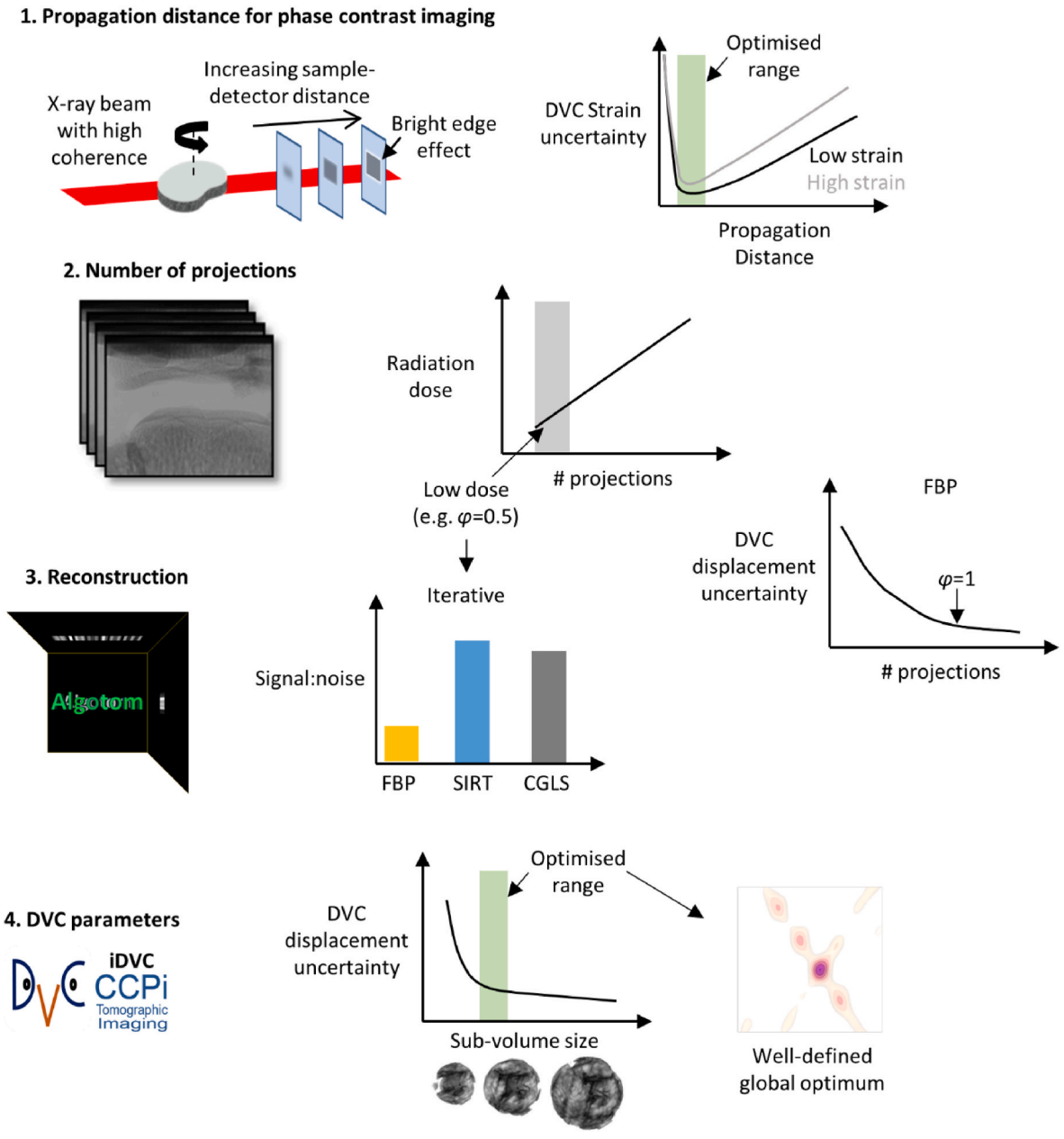

Optimising low dose	Optimising DVC accuracy
• Larger strain steps, lower number of scans • Projections < 0.5 (φ) • Iterative reconstruction • High density of sub-volume points	• Smaller strain steps, higher number of scans • Projections > 1 (φ) • FBP reconstruction (lower computation vs iterative)
Always optimise propagation distance and sub-volume size	

Fig. 7. Summary of optimising soft tissue *in situ* tomography. 1. Propagation distance should be set as short as possible to resolve small scale features. There is an acceptable range in which the accuracy of DVC results is not affected. Radiation exposure can be further lowered by using larger strain steps and therefore lower number of total scans but with a decrease in DVC accuracy particularly at larger propagation distances. **2 & 3.** Fewer projections can be used to lower radiation dose but with a trade off in DVC accuracy. Although iterative reconstruction methods for lower number of projections increases computation (see Suppl. info. for computation times), they can be used to increase signal-to-noise ratio and lower DVC displacement uncertainty. **4.** Optimising DVC parameters such as sub-volume size is essential.

Data availability

Data will be made available on request.

Acknowledgements

CMD/PDL are grateful for the support from UK-EPSRC (EP/V011006/1). PDL acknowledges funding from Royal Academy of Engineering Chair in Emerging Technologies (CiET) (1819/10). Facilities and research support were provided by the Diamond-Manchester Branchline I13-2 and the Research Complex at Harwell. Diamond Light Source beam time was provided under proposal MT19322. This research used a resource of the National Synchrotron Light Source II, a U.S. Department of Energy (DOE) Office of Science User Facility, operated for the DOE Office of Science by Brookhaven National Laboratory under Contract No. DE-SC0012704. Tomography data used in this manuscript has been published in (Disney et al., 2022).

Appendix A. Supplementary data

Supplementary data to this article can be found online at https://doi.org/10.1016/j.jmbbm.2022.105579.

References

Abidin, A.Z., Deng, B.T., Dsouza, A.M., Nagarajan, M.B., Coan, P., Wismuller, A., 2018. Deep transfer learning for characterizing chondrocyte patterns in phase contrast X-Ray computed tomography images of the human patellar cartilage. Comput. Biol. Med. 95, 24–33.

Arhatari, B.D., Stevenson, A.W., Abbey, B., Nesterets, Y.I., Maksimenko, A., Hall, C.J., Thompson, D., Mayo, S.C., Fiala, T., Quiney, H.M., Taba, S.T., Lewis, S.J., Brennan, P.C., Dimmock, M., Hausermann, D., Gureyev, T.E., 2021. X-Ray Phase-Contrast Computed Tomography for Soft Tissue Imaging at the Imaging and Medical Beamline (IMBL) of the Australian Synchrotron. Applied Sciences-Basel vol. 11.

Arora, H., Nila, A., Vitharana, K., Sherwood, J.M., Nguyen, T.-T.N., Karunaratne, A., Mohammed, I.K., Bodey, A.J., Hellyer, P.J., Overby, D.R., 2017. Microstructural consequences of blast lung injury characterized with digital volume correlation. Frontiers in Materials 4, 41.

Barth, H.D., Zimmermann, E.A., Schaible, E., Tang, S.Y., Alliston, T., Ritchie, R.O., 2011. Characterization of the effects of x-ray irradiation on the hierarchical structure and mechanical properties of human cortical bone. Biomaterials 32, 8892–8904.

Boas, F.E., Fleischmann, D., 2011. Evaluation of two iterative techniques for reducing metal artifacts in computed tomography. Radiology 259, 894–902.

Borg, L., Sporring, J., Dam, E.B., Dahl, V.A., Dyrby, T.B., Feidenhans'L, R., Dahl, A.B., Pingel, J., 2019. Muscle fibre morphology and microarchitecture in cerebral palsy patients obtained by 3D synchrotron X-ray computed tomography. Comput. Biol. Med. 107, 265–269.

Burvall, A., Lundström, U., Takman, P.A., Larsson, D.H., Hertz, H.M., 2011. Phase retrieval in X-ray phase-contrast imaging suitable for tomography. Opt Express 19, 10359–10376.

Cianciosi, F., Buisson, A.-L., Tafforeau, P., VAN Vaerenbergh, P., 2021. BM18, the New ESRF-EBS Beamline for Hierarchical Phase-Contrast Tomography. 11th Mechanical Engineering Design of Synchrotron Radiation Equipment and Instrumentation (MEDSI'20). July 2021. JACOW Publishing, Chicago, IL, USA, pp. 24–29. Geneva, Switzerland, 1-5.

Cicek, E., 2016. Effect of X-ray irradiation on articular cartilage mechanical properties. Acta Phys. Pol., A 129, 200–202.

Croton, L.C., Morgan, K.S., Paganin, D.M., Kerr, L.T., Wallace, M.J., Crossley, K.J., Miller, S.L., Yagi, N., Uesugi, K., Hooper, S.B., 2018. In situ phase contrast X-ray brain CT. Sci. Rep. 8, 1–12.

Dall'Ara, E., Bodey, A., Isaksson, H., Tozzi, G., 2022. A practical guide for in situ mechanical testing of musculoskeletal tissues using synchrotron tomography. J. Mech. Behav. Biomed. Mater., 105297

Dall'Ara, E., Peña-Fernández, M., Palanca, M., Giorgi, M., Cristofolini, L., Tozzi, G., 2017. Precision of digital volume correlation approaches for strain analysis in bone imaged with micro-computed tomography at different dimensional levels. Frontiers in Materials 4.

Disney, C., Eckersley, A., Mcconnell, J., Geng, H., Bodey, A., Hoyland, J., Lee, P., Sherratt, M., Bay, B., 2019. Synchrotron tomography of intervertebral disc deformation quantified by digital volume correlation reveals microstructural influence on strain patterns. Acta Biomater. 92, 290–304.

Disney, C., Lee, P., Hoyland, J., Sherratt, M., Bay, B., 2018. A review of techniques for visualising soft tissue microstructure deformation and quantifying strain Ex Vivo. J. Microsc. 272, 165–179.

Disney, C., Madi, K., Bodey, A., Lee, P., Hoyland, J., Sherratt, M., 2017. Visualising the 3D microstructure of stained and native intervertebral discs using X-ray microtomography. Sci. Rep. 7, 1–11.

Disney, C., Mo, J., Eckersley, A., Bodey, A., Hoyland, J., Sherratt, M., Pitsillides, A., Lee, P., Bay, B., 2022. Regional variations in discrete collagen fibre mechanics within intact intervertebral disc resolved using synchrotron computed tomography and digital volume correlation. Acta Biomater. 138, 361–374.

Einarsson, E., Pierantoni, M., Novak, V., Svensson, J., Isaksson, H., Englund, M., 2022. Phase-contrast enhanced synchrotron micro-tomography of human meniscus tissue. Osteoarthritis Cartilage 30, 1222–1233.

Fernández, M.P., Cipiccia, S., Dall'Ara, E., Bodey, A.J., Parwani, R., Pani, M., Blunn, G. W., Barber, A.H., Tozzi, G., 2018. Effect of SR-microCT radiation on the mechanical integrity of trabecular bone using in situ mechanical testing and digital volume correlation. J. Mech. Behav. Biomed. Mater. 88, 109–119.

Gates, M., Gonzalez, J., Lambros, J., Heath, M.T., 2015. Subset refinement for digital volume correlation: numerical and experimental applications. Exp. Mech. 55, 245–259.

Häggmark, I., Vågberg, W., Hertz, H.M., Burvall, A., 2017. Comparison of quantitative multi-material phase-retrieval algorithms in propagation-based phase-contrast X-ray tomography. Opt Express 25, 33543–33558.

Hahn, D., Thibault, P., Bech, M., Stockmar, M., Schleede, S., Zanette, I., Rack, A., Weitkamp, T., Sztrokay, A., Schlossbauer, T., Bamberg, F., Reiser, M., Pfeiffer, F., 2012. Numerical comparison of X-ray differential phase contrast and attenuation contrast. Biomed. Opt Express 3, 1141–1148.

Hehn, L., Morgan, K., Bidola, P., Noichl, W., Gradl, R., Dierolf, M., Noël, P.B., Pfeiffer, F., 2018. Nonlinear statistical iterative reconstruction for propagation-based phase-contrast tomography. APL bioengineering 2, 016105.

Henke, B.L., Gullikson, E.M., Davis, J.C., 1993. X-ray interactions: photoabsorption, scattering, transmission, and reflection at E= 50-30,000 eV, Z= 1-92. Atomic Data Nucl. Data Tables 54, 181–342.

Kak, A.C., Slaney, M., 2001. Principles of Computerized Tomographic Imaging. SIAM.

Lindburg, C.A., Willey, J.S., Dean, D., 2013. Effects of low dose X-ray irradiation on porcine articular cartilage explants. J. Orthop. Res. 31, 1780–1785.

Lovric, G., Barre, S.F., Schittny, J.C., Roth-Kleiner, M., Stampanoni, M., Mokso, R., 2013. Dose optimization approach to fast X-ray microtomography of the lung alveoli. J. Appl. Crystallogr. 46, 856–860.

Madi, K., Staines, K.A., Bay, B.K., Javaheri, B., Geng, H., Bodey, A.J., Cartmell, S., Pitsillides, A.A., Lee, P.D., 2019. In situ characterization of nanoscale strains in loaded whole joints via synchrotron X-ray tomography. Nature biomedical engineering 1–12.

Pacureanu, A., Langer, M., Boller, E., Tafforeau, P., Peyrin, F., 2012. Nanoscale imaging of the bone cell network with synchrotron X-ray tomography: optimization of acquisition setup. Med. Phys. 39, 2229–2238.

Palanca, M., Tozzi, G., Cristofolini, L., Viceconti, M., Dall'Ara, E., 2015. Three-dimensional local measurements of bone strain and displacement: comparison of three digital volume correlation approaches. J. Biomech. Eng. 137.

Pan, B., Wang, B., 2020. Some recent advances in digital volume correlation. Opt Laser. Eng. 135.

Pierantoni, M., Barreto, I.S., Hammerman, M., Verhoeven, L., Tornquist, E., Novak, V., Mokso, R., Eliasson, P., Isaksson, H., 2021. A quality optimization approach to image Achilles tendon microstructure by phase-contrast enhanced synchrotron micro-tomography. Sci. Rep. 11.

Rawson, S.D., Maksimcuka, J., Withers, P.J., Cartmell, S.H., 2020. X-ray computed tomography in life sciences. BMC Biol. 18.

Sartori, J., Köhring, S., Bruns, S., Moosmann, J., Hammel, J.U., 2021. Gaining insight into the deformation of achilles tendon entheses in mice. Adv. Eng. Mater. 23, 2100085.

Strotton, M.C., Bodey, A.J., Wanelik, K., Darrow, M.C., Medina, E., Hobbs, C., Rau, C., Bradbury, E.J., 2018. Optimising complementary soft tissue synchrotron X-ray microtomography for reversibly-stained central nervous system samples. Sci. Rep. 8, 1–18.

Tavana, S., Clark, J.N., Prior, J., Baxan, N., Masouros, S.D., Newell, N., Hansen, U., 2020. Quantifying deformations and strains in human intervertebral discs using Digital Volume Correlation combined with MRI (DVC-MRI). J. Biomech. 102.

Tozzi, G., Peña Fernández, M., Davis, S., Karali, A., Kao, A.P., Blunn, G., 2020. Full-Field Strain Uncertainties and Residuals at the cartilage-bone interface in unstained tissues using propagation-based phase-contrast XCT and digital volume correlation. Materials 13, 2579.

VAN Aarle, W., Palenstijn, W.J., Cant, J., Janssens, E., Bleichrodt, F., Dabravolski, A., DE Beenhouwer, J., Batenburg, K.J., Sijbers, J., 2016. Fast and flexible X-ray tomography using the ASTRA toolbox. Opt Express 24, 25129–25147.

Vo, N.T., Atwood, R.C., Drakopoulos, M., 2015. Radial lens distortion correction with sub-pixel accuracy for X-ray micro-tomography. Opt Express 23, 32859–32868.

Vo, N.T., Atwood, R.C., Drakopoulos, M., 2018. Superior techniques for eliminating ring artifacts in X-ray micro-tomography. Opt Express 26, 28396–28412.

Vo, N.T., Atwood, R.C., Drakopoulos, M., Connolley, T., 2021. Data processing methods and data acquisition for samples larger than the field of view in parallel-beam tomography. Opt Express 29, 17849–17874.

Vo, N.T., Atwood, R.C., Moser, H.O., Lee, P.D., Breese, M.B., Drakopoulos, M., 2012. A fast-converging iterative method for X-ray in-line phase contrast tomography. Appl. Phys. Lett. 101, 224108.

Walsh, C., Tafforeau, P., Wagner, W., Jafree, D., Bellier, A., Werlein, C., Kühnel, M., Boller, E., Walker-Samuel, S., Robertus, J., 2021. Imaging intact human organs with

local resolution of cellular structures using hierarchical phase-contrast tomography. Nat. Methods 18, 1532–1541.
Wearne, L.S., Rapagna, S., Taylor, M., Perilli, E., 2022. Micro-CT scan optimisation for mechanical loading of tibia with titanium tibial tray: a digital volume correlation zero strain error analysis. J. Mech. Behav. Biomed. Mater. 134.
Zeller-Plumhoff, B., Roose, T., Katsamenis, O.L., Mavrogordato, M.N., Torrens, C., Schneider, P., Clough, G.F., 2017. Phase contrast synchrotron radiation computed tomography of muscle spindles in the mouse soleus muscle. J. Anat. 230, 859–865.